JMEPEG (2009) 18:594–599
DOI: 10.1007/s11665-009-9493-8

1059-9495/$19.00

Thermomechanical Properties of Porous NiTi Alloy Produced by SHS

P. Bassani, P. Giuliani, A. Tuissi, and C. Zanotti

(Submitted October 24, 2008; in revised form April 21, 2009)

Samples obtained from relatively large powders (<150 μm), with total porosity in the range 30-68%, were characterized mainly from a morphological point of view. Total porosity, as well as pore size, shape and distribution, was analyzed. Sample microstructure was also investigated, indicating that the main phase produced during the self-propagating high-temperature synthesis (SHS) reaction is Ti reach NiTi phase, as confirmed by calorimetric analyses. Moreover, the presence of secondary phases, suggested by the low transformation enthalpy, was confirmed by SEM observations. In fact, EDS microanalyses and EBSD mapping helped in the identification of such secondary phases, such as Ni_3Ti, Ti_2Ni and $Ti_4Ni_2O_x$. Other samples were successively produced starting from the same powders but introducing a different powder compression methodology and operating conditions. In this way, the obtained samples showed higher porosity featured by more uniform size, shape and distribution while, from a micro-structural point of view, no significant differences were observed. Mechanical compression tests were carried out at room temperature and, on selected samples, also above A_f in order to highlight the influence of pore shape and distribution. Results obtained at room temperature show that the mechanical properties decrease with the porosity augmentation. For higher temperatures, the samples presented a pseudoelastic behavior. Dilatometric tests were also performed and the results well indicated the martensite to austenite transformation at the same temperature showed by the DSC analyses. Thermal analysis was completed by evaluating the thermal diffusivity temperature and porosity dependence using an experimental-numerical approach especially developed.

Keywords advanced characterization, intermetallics, mechanical testing, metallography

1. Introduction

Porous NiTi has been intensively studied in the last years due to the high interest as a possible material for biomedical applications; it offers good biocompatibility, mechanical properties closer than other metallic material to those of bone, shape recovery behavior that can help in insertion operation, excellent compatibility with magnetic resonance and computer tomography scanning. Several studies have been performed on mechanical properties and corrosion characteristics of bulk and porous NiTi (Ref 1, 2) in view of these field of applications. Interest in porous NiTi is still acute, due to continuing research on biomedical field application/optimization but also due to possible application as vibration dampers or shock absorber.

For the latter application not only mechanical behavior is important but also a comprehensive view of thermomechanical properties is of interest. Self-propagating high-temperature synthesis (SHS) was proposed as a suitable route for the production of porous NiTi alloys with different degree of porosity. In fact, by controlling the compaction procedure of the starting powders and some parameters such as mixing ratio of Ni and Ti powders, powder size and shape, sample size and shape, it is possible to adjust the product porosity. Moreover, the operating conditions driving the SHS process (ignition technique, preheating temperature, atmosphere and gas (argon) pressure) can influence the characteristics of the final porosity. In order to obtain samples featured with greater porosity, a variation in powder processing was introduced: the starting material was loaded inside a ceramic tube and then reacted. Microstructural and thermomechanical tests were performed in order to characterize the properties of the samples produced and also to verify if any abrupt variation occurred during the SHS procedure.

2. Experimental

It is necessary to define the sample porosity, ρ, used for presenting our results.

$$\rho\% = \left(1 - (\rho_p/\rho_f)\right) * 100$$

where ρ_f is the density of the full dense while ρ_p is the density of the porous NiTi.

Samples of porous NiTi were prepared by the SHS technique starting from relatively large size powders (~150 μm). Powders were dry mixed, with equiatomic

This article is an invited paper selected from presentations at Shape Memory and Superelastic Technologies 2008, held September 21-25, 2008, in Stresa, Italy, and has been expanded from the original presentation.

P. Bassani and **A. Tuissi**, National Research Council, Institute for Energetics and Interphases, Lecco, Italy; and **P. Giuliani** and **C. Zanotti**, National Research Council, Institute for Energetics and Interphases, Milan, Italy. Contact e-mail: p.bassani@ieni.cnr.it.

composition of Ni and Ti, compacted in cylindrical shape with different compacting pressure and then reacted, obtaining porosity up to 45%. Details regarding the sample preparation by SHS technique can be found in Ref 3.

In order to increase the final porosity of the reacted sample, another preparation route was optimized: after mixing, the powders were placed inside a ceramic tube and only slightly shacked or pressed. Porosities in the range 48-68% were thereby obtained.

Tests were replicated in order to verify the repeatability of our results and to obtain various samples with the same characteristics for subsequent tests.

Selected samples were prepared for porosity measurements and microstructural investigations: the cylinders obtained were sectioned longitudinally in two parts: one was further sectioned longitudinally at ½ R and the other was sectioned perpendicularly to the cylinder axis, obtaining three transverse sections. Surfaces were first roughly polished for image analysis, and after that, selected sections were cold mounted in epoxy resin, polished with diamond paste and finally with colloidal silica, in order to obtain surfaces suitable for EDS and EBSD (Electron Back Scattered Diffraction) analyses, performed with a LEO 1430 SEM equipped with INCA Energy 300 and INCA Crystal detectors. For details on EBSD sample preparation and observation see Ref 4. DSC analyses were carried out on specimen cut with a metallographic diamond saw from different position in the samples. Analyses were performed with a Seiko DSC, with heating/cooling rate of 10 °C/min, on specimen of about 30 mg in mass.

Samples for thermal diffusivity evaluation, dilatometric and mechanical tests were obtained simply by machining top and bottom surfaces of the products in order to obtain cylinders approximately 12 mm height and flat, parallel bases. Thermal diffusivity was estimated using a simple, 1D, numerical code that simulates the heat transfer phenomena in a multi-layers cylindrical sample. Thermal diffusivity dependence on temperature and porosity has been changed in order to reproduce experimental data concerning heating and cooling transients. The experimental procedure and the numerical approach are described in Ref 5. Mechanical tests were performed according to ASTM E9-89a (Ref 6), on an MTS 810 universal testing machine, equipped with a 250 kN force transducer. Test to failure was performed at room temperature, while cyclic loading/unloading with increasing deformation up to 6% was performed both at room temperature and at 110-120-130 °C, according to ASTM E209-00 (Ref 7). In all cases test parameters were selected in order to have a constant strain rate of about 10^{-6} [s^{-1}].

3. Results and Discussion

3.1 Microstructural Characterization

By employing the SHS route we were able to produce samples with porosity ranging from 10 to 68%. For porosity less than 45%, pores are often not interconnected, and especially the larger ones lie on planes parallel to the specimen base. By increasing porosity a significant interconnection is obtained, without preferential orientation. Image analyses of the percent of porosity on the various section of specimen confirmed substantial homogeneous distribution of the resultant

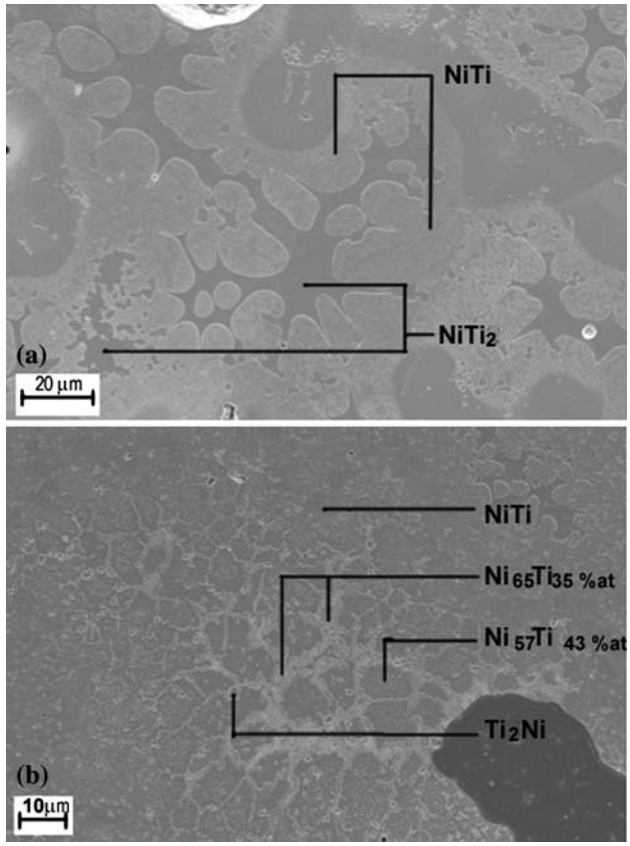

Fig. 1 SEM images with indication of EDXS results on typical morphology: (a) rounded concave agglomerates (mainly Ti_2Ni or $Ti_4Ni_2O_x$); (b) branched agglomerates (mainly Ni_3Ti and NiTi)

pores. The pore morphology of samples produced by SHS has been already reported by the authors (see Ref 4).

Optical microscope investigations on microstructure did not show any differences inside the specimens and between samples of differing total porosity. In all cases, in a matrix of NiTi, the presence of secondary phases was observed, mainly grouped in small region with two main morphologies (Fig. 1a, b). EDS analyses allowed us to identify possible candidates for the observed structure. EBSD analyses provided further information on structure and eventual grain size of the observed phases. In one case (Fig. 1a and 2a), rounded, concave particles are constituted mainly by Ti_2Ni or $Ti_4Ni_2O_x$. In the other case branched structures resulted in a mix of eutectic constituent formed by Ni_3Ti and NiTi, mixed with Ti_2Ni or $Ti_4Ni_2O_x$, as polygonal particles (Fig. 1b and 2b). It was not possible with the investigations brought about to define the oxygen content of the $Ti_4Ni_2O_x$ particles: so it was preferred not to make any assumption about the exact composition of those phases.

3.2 DSC Investigations

Calorimetric analyses results are summarized in Fig. 3 and 4. As indicated in Fig. 3, transformation temperatures are substantially independent of total porosity and can be associated with a Ti-rich NiTi matrix. Enthalpy values shown in Fig. 4 and estimated using small samples (20-30 mg in mass) are less than a corresponding annealed bulk material (26.1 J/g). A correlation between transformation enthalpies and porosity, referred to the sample having greater size, can only be argued.

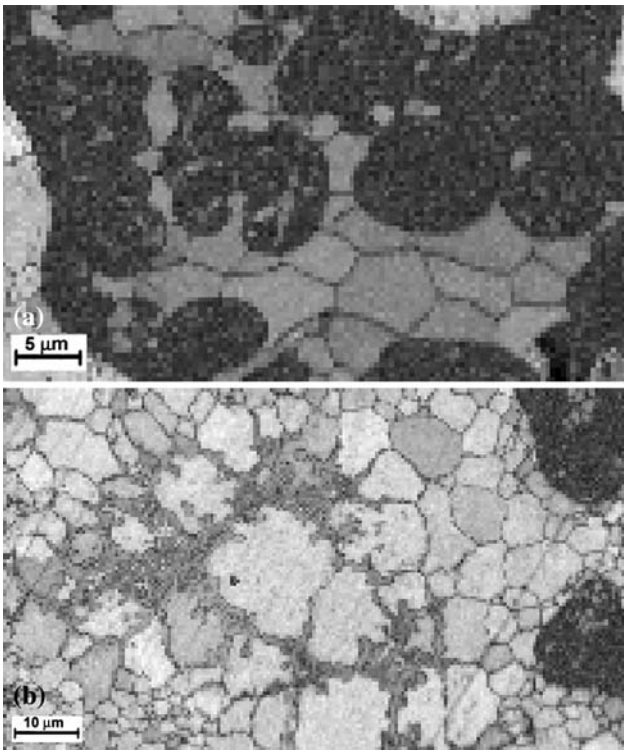

Fig. 2 Pattern quality map obtained from EBSD analysis on two regions with morphology similar to those of Fig. 1. Strict correspondence between quality pattern and phase identification maps (not reported) was observed. Ti_2Ni (medium dark grey area), Ni rich-NiTi (light grey), martensite matrix (dark grey). Mapped area: (a) 50 × 28 µm; (b) 100 × 60 µm

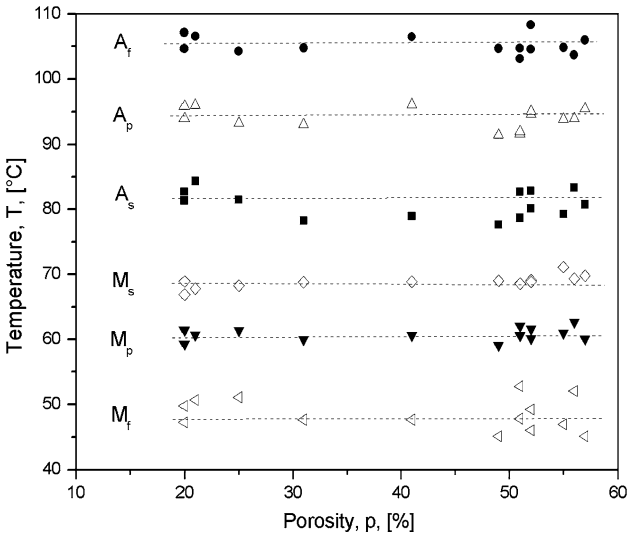

Fig. 3 DSC transformation temperatures for samples with different porosity: no porosity dependence can be argued

In fact, the general trend of the data indicates that transformation enthalpy increases slightly with the sample porosity augmentation. Heating/cooling enthalpies fall in a range from 4 to 8 J/g and show minimum values for porosity of about 30%. This behavior is in agreement with results reported in Ref 8, in which the porosity ranged from 25 to 45%.

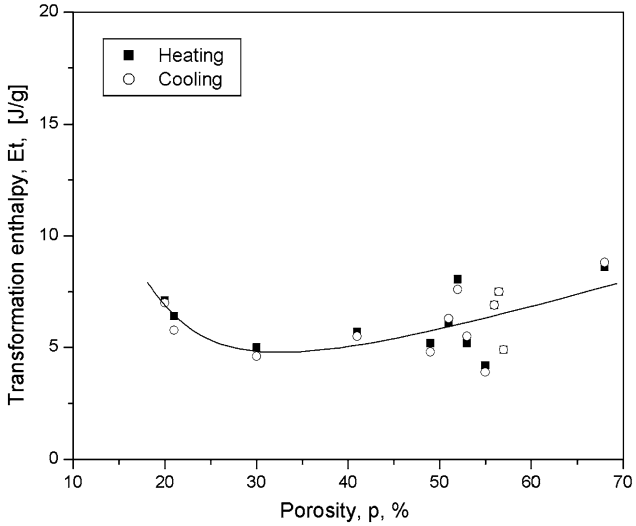

Fig. 4 DSC transformation enthalpies as a function of porosity

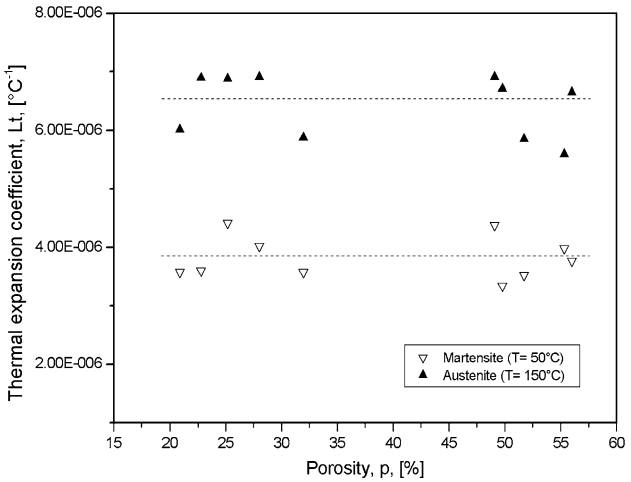

Fig. 5 Linear expansion coefficient for martensitic and austenitic conditions vs. porosity

The observed scatter can be attributed in part to local inhomogeneities, with a greater/lesser presence of secondary phases. The low mean value can be related in part only to the presence of secondary phases that subtract mass to transformation. In particular, as observed with the help of EDS-EBSD analyses, also Ni-rich NiTi regions were observed that did not result in any calorimetric event, evidencing a stabilized austenitic structure.

3.3 Dilatometric Tests

Transformation temperatures from dilatometric tests mimic very well those results from the more commonly used DSC analysis. An attempt to derive linear expansion coefficients above and below the transformation region has been performed. Unfortunately only a qualitative result could be obtained. Scattered values were obtained not only from one sample to another with the same porosity, but also during repeated tests on the same sample. An overview of the results is reported in Fig. 5: no correlation with the porosity was observed, and an

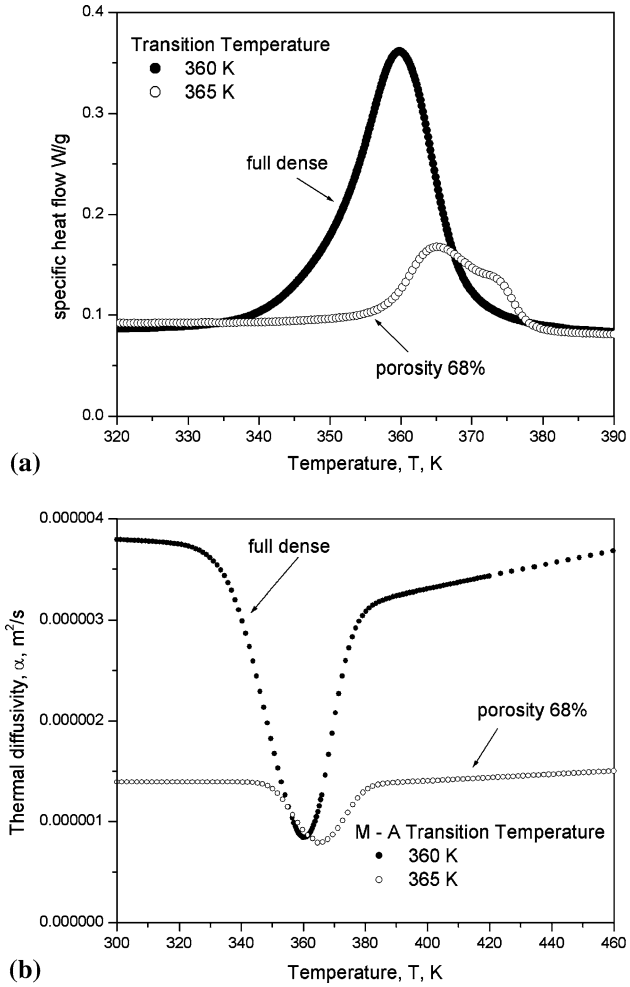

Fig. 6 Comparison between heating ramp of DSC analyses on bulk and porous NiTi (a) and corresponding thermal diffusivity (b)

average value around 6.0×10^{-6} and 3.7×10^{-6} for austenite and martensite respectively so derived is in good agreement with literature value for bulk material.

3.4 Thermal Diffusivity Evaluation

In the following, a general definition of thermal diffusivity is reported and the effective thermal diffusivity in the case of porous matter is explained.

$$\text{Thermal diffusivity: } \alpha(T) = K_c(T)/(C_p(T) * \rho)$$

where $K_c(T)$ is the thermal conductivity, $C_p(T)$ the heat capacity and ρ the density.

$$\text{Effective thermal diffusivity: } \alpha_e = \alpha_s + \alpha_f + \alpha_r$$

where α_s concerns the solid (NiTi), α_f the fluid (argon) and α_r the radiative transport phenomena inside the porous sample.

Generally, heat transfer phenomena, associated to the presence of gas (argon) in the pores, is negligible at low operating pressure (0.1 MPa). Also, no effect for the temperature increasing has to be taken into account when porosity was less than ~90%.

On the other hand, of more importance is the radiative transport phenomenon inside the porous samples. In fact, the

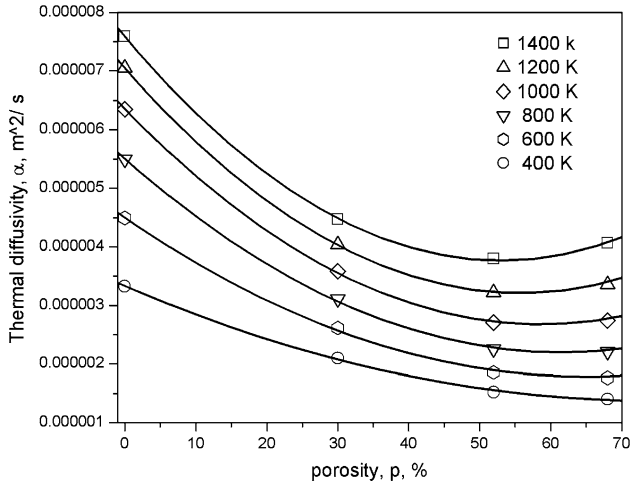

Fig. 7 Thermal diffusivity vs. porosity for different temperatures

heat transfer by radiation depends on the random, open-cell porosity distribution (Ref 9-11) and this influence become greater and greater with increased porosity and temperature. Thermal diffusivities were therefore estimated based on these considerations and in accord with the DSC data obtained for porous samples.

For what concerns DCS data a comparison between full dense and porous samples is reported in Fig. 6(a) (heating case), indicating that the peak value decreases as porosity increases. This occurrence has been taken into account carrying out simulations and results, presented in Fig. 6(b), were obtained. This figure illustrates that the effective thermal diffusivity of porous sample is lower with respect to the value of the full dense material but the minimum, reached close to the transition temperature, is essentially the same.

Finally, data obtained by the numerical computations, relevant samples characterized by different porosity values (30, 48 and 68%) are reported and compared with the full dense data in Fig. 7.

The general trend of the reported curves indicates that the α decreases with the porosity increase while it increases with the temperature augmentation.

Thermal diffusivity dependence on porosity indicates that, at low temperature (400 K), it decreases with the porosity augmentation, while in the case of high temperature (1400 K) this behavior change approaching the porosity value of 50%. As mentioned above, this occurrence can be explained considering that radiative transport phenomena depend on the random open-cell porous samples and their effect becomes larger and larger with porosity and temperature increase.

3.5 Mechanical Tests

The results of compression until failure, as expected, confirmed that increasing the porosity reduces the mechanical properties of the material: maximum stress values of about 350 MPa were reached for samples with approximately 30% porosity, while samples with over 50% porosity hardly achieved 100 MPa. This effect was in part expected, as increasing porosity results in a reduction of resistant cross-sectional area. Not only the degree of porosity but, of course, the morphology of the void influences the mechanical results: a more homogeneous distribution of voids could contribute to a

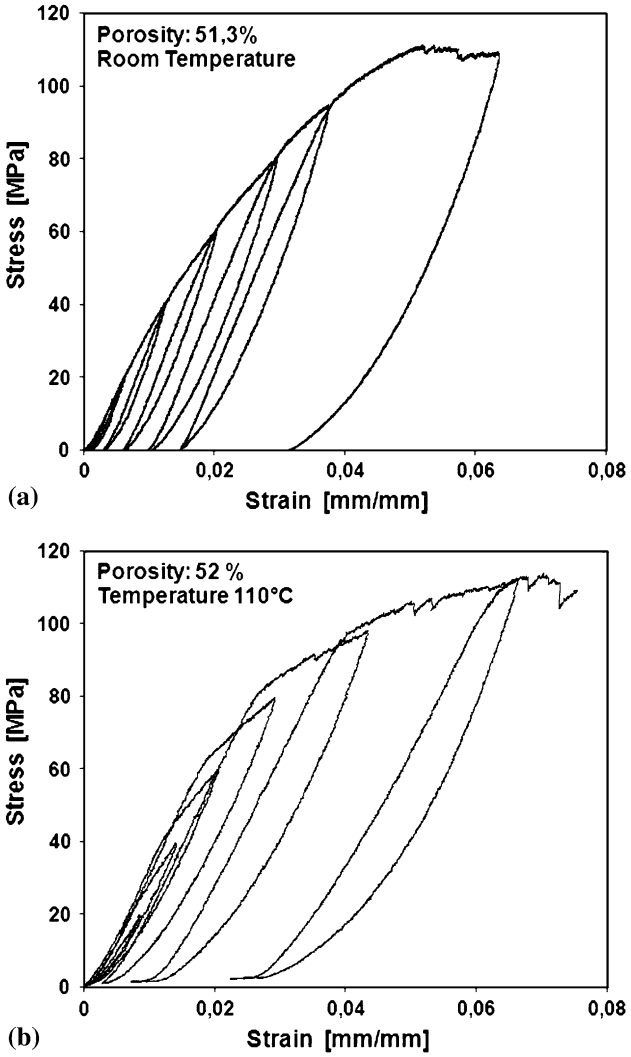

Fig. 8 Cyclic compression curves on two samples with same porosity at (a) room temperature and (b) 110 °C. In the latter condition, the sample exhibits pseudoelastic effect

better distribution of force on the section of the sample, with respect to samples with a localized concentration of voids, resulting in improved mechanical properties. Moreover, failure was observed to occur always as a localized collapsing on a plane roughly at 30° from horizontal. The previous assumption, together with the observation of localized deformation region in failed specimens, can justify some irregularities in stress-porosity dependence of mechanical behavior.

Samples with approximately 53% porosity were also tested with cyclic loading/unloading, at room temperature and at 110, 120 and 130 °C in order to check the presence of pseudo-elastic effects. Typical results are reported in Fig. 8(a) and (b). At room temperature, the specimens suffered progressive accumulation of deformation, with reloading curves copying the previous unloading curve, while at higher temperature a typical recovery during unloading was observed. The maximum recovery for each unloading cycle of about 0.5% is observed at 110 °C. At higher temperatures the strain recovery was reduced. This is reasonable because with increasing the temperature the permanent deformation of austenite is favored with respect to martensite-induced formation. Moreover, it should be noted that the NiTi matrix has not been subjected to any treatment with the aim of increasing the superelastic window.

4. Conclusions

SHS technique can be employed satisfactorily for producing NiTi porous sample with tailored porosity.

Calorimetric and dilatometric measurements show no dependence from degree of porosity, in agreement with microstructural observation, that reported common features in all samples. Mechanical properties were clearly affected by the degree of porosity; nonetheless, pseudo-elastic behavior was observed also for higher porosity.

Thermal diffusivity measurements on the contrary show a clear dependence not only on temperature, but also on porosity: at lower temperature thermal diffusivity decreases, due to reduction of material area available for conductive thermal transfer. At higher temperatures, up to 53% of porosity, reduction was observed, while at greater porosity thermal diffusivity increases due to the increasing contribute of radiative transmission through interconnected porosity inside the sample.

Further optimization of the SHS technique could be obtained with increased transforming fraction and further control over porosity size and distribution. As an SHS sample's porosity is related, among other parameters, to the initial porosity of the compacted powders, in order to obtain greater values of porosity looser powders need to be employed, with clear limitation in handling procedures. Optimization of SHS techniques applied to confined loose powders resulted in up to 68% porous NiTi samples. This technique could lead to the production of near net shape components for small to medium component application.

Acknowledgment

The authors thank Mr. G. Negro for technical support during experimental tests and numerical analyses.

References

1. S. Shabalovskaya, Surface, Corrosion and Biocompatibility Aspects of Nitinol as an Implant Material, *Biomed. Mater. Eng.*, 2002, **12**, p 69–109
2. A. Bansiddhi, T.D. Sargeant, S.I. Stupp, and D.C. Dunand, Porous NiTi for Bone Implants: A Review, *Acta Biomater.*, 2008, **4**, p 773–782
3. C. Zanotti, P. Giuliani, P. Bassani, F. Passaretti, and A. Tuissi, Characterization of Porous NiTi Alloys Produced by SHS, *Proceedings of SMST 2006 International Conference on Shape Memory and Superelastic Technologies*, B. Berg, M.R. Mitchell, and J. Proft, Ed., May 7-11, 2006 (Asilomar, Pacific Grove, CA), p 373–380
4. A. Tuissi, P. Bassani, and F. Passaretti, EBSD Microstructural Characterization of Ni50.8Ti49.2 Shape Memory Alloy, *Proceedings of SMST 2006 International Conference on Shape Memory and Superelastic Technologies*, B. Berg, M.R. Mitchell, and J. Proft, Ed., May 7-11, 2006 (Asilomar, Pacific Grove, CA), p 741–748
5. C. Zanotti, P. Giuliani, G. Riva, A. Tuissi, and A. Chrysanthou, Thermal Diffusivity of Ni-Ti SMAs, *J. Alloys Compd.*, 2009, **473**, p 231–237. doi:10.1016/j.jallcom.2008.05.040
6. Standard Test Method of Compression Testing of Metallic Materials at Room Temperature. ASTM (American Society for Testing and Materials) E9-89a (Reapproved 2000). ASTM International, 2000

7. Standard Practice for Compression Test of Metallic Materials at Elevated Temperatures with Conventional or Rapid Heating Rates and Strain Rates. ASTM (American Society for Testing and Materials) E209-00. ASTM International, 2000
8. B. Yuan, X.P. Zhang, C.Y. Chung, and M. Zhua, The Effect of Porosity on Phase Transformation Behavior of Porous Ti-50.8 at.% Ni Shape Memory Alloys Prepared by Capsule-Free Hot Isostatic Pressing, *Mater. Sci. Eng. A*, 2006, **438–440**, p 585–588
9. C.Y. Zhao, S.A. Tassou, and T.J. Lu, Analytical Considerations of Thermal Radiation in Cellular Metal Foams with Open Cells, *Int. J. Heat Mass Transf.*, 2008, **51**, p 929–940
10. M. Wang and N. Pan, Modeling and Prediction of the Effective Thermal Conductivity of Random Open-Cell Porous Foams, *Int. J. Heat Mass Transf.*, 2008, **51**, p 1325–1331
11. X. Huai, W. Wang, and Z. Li, Analysis of Effective Thermal Conductivity of Fractal Porous Media, *Appl. Therm. Eng.*, 2007, **27**, p 2815–2821